

# Changes in freezing-thawing index and soil freeze depth over the Heihe River Basin, western China

Xiaoqing Peng,<sup>1</sup> Tingjun Zhang,<sup>1,\*</sup> Bin Cao,<sup>1</sup> Qingfeng Wang,<sup>2</sup> Kang Wang,<sup>1</sup> Wanwan Shao,<sup>1</sup> and Hong Guo<sup>1</sup>

<sup>1</sup>Key Laboratory of Western China's Environmental Systems (Ministry of Education), College of Earth and Environmental Sciences, Lanzhou University, Lanzhou, Gansu 730000, China

<sup>2</sup>Cold and Arid Regions Environmental and Engineering Research Institute, Chinese Academy of Sciences, Lanzhou, Gansu 730000, China

\*Corresponding author's email: [tjzhang@lzu.edu.cn](mailto:tjzhang@lzu.edu.cn)

## ABSTRACT

Freezing/thawing index is an important indicator of climate change, and can be used to estimate depths of the active layer and seasonally frozen ground (SFG). Using the mean monthly grid air temperature from 2000 to 2009 as well as daily air and ground surface temperatures from 12 meteorological stations across the Heihe River Basin, this study investigated spatial and temporal variability of the freezing/thawing index and seasonal soil freeze depth. The mean annual air temperature increased at a rate of  $0.35\text{ }^{\circ}\text{C decade}^{-1}$  from 1960 to 2013, or approximately  $1.9\text{ }^{\circ}\text{C}$  for the 54-year period. We found that the freezing index (FI) showed a decreasing trend over the study area, while the thawing index (TI) had an increasing trend. Changes in both FI and TI are consistent with an increasing mean annual air temperature. The TI and freezing  $n$ -factor ( $n_f$ ) decrease with elevation increase, while FI and thawing  $n$ -factor ( $n_t$ ) increase with elevation. Soil potential seasonal freezing depth was primarily between 1.5 and 2.5 m in permafrost regions. However, the soil maximum freezing depth is below 2.5 m in SFG region.

## INTRODUCTION

In recent years, global climate warming and unusual weather patterns have raised public concerns. Recent research on general circulation models (GCMs) indicate that global warming will continue and that its amplitude will increase during the 21st century (Susan, 2007). Because frozen ground is generally found in cold climates, the effect of climate warming on frozen ground is a great concern for the scientific research community and society (Stocker et al., 2013, Ch. 4). Climate warming can cause permafrost degradation, including a thickening of the active layer, expansion of taliks, and the disappearance of sporadic permafrost (Lunardini, 1996; Cheng and Xu, 1993; Wu et al., 2008; Zhang,

2012). During previous research, significant efforts have been devoted to permafrost-related studies. However, despite the vast extent and importance of seasonally frozen ground (SFG), it has received much less attention (Shiklomanov, 2012). Changes in SFG have important impacts on the surface energy balance, the hydrologic cycle, carbon exchange between the atmosphere and the land surface, plant growth, and ecosystems as a whole (Zhang et al., 2005). Soil freeze depth was a key factor reflecting changes of SFG. Soil freeze-thaw depths are important information for building and transport design in cold regions (Steurer, 1996; Jingkang and Guisheng, 2000; Li and Wu, 2004; Vermette and Christopher, 2008) and are also important indicators of climate change (Frauenfeld et al., 2004).

Freezing/thawing indices are important factors that reflect changes in the cryosphere (Nelson, 2003). In general, there are two types of freezing/thawing indices: the surface freezing index (0 cm above the ground) and the air freezing index (150–200 cm above the ground). The freeze-thaw index has been used to accurately predict and map permafrost distribution (Nelson and Outcalt, 1987). A freeze index model, as a statistical model, has been used to assess permafrost and SFG distribution (Nelson and Outcalt, 1987) and was successfully used to simulate and predict small-scale permafrost distributions in high-latitude regions. However, for larger scales, such as the Tibetan Plateau, model outputs for frozen ground distribution have been less accurate, mainly due to a lack of accurate regional-scale data sets (Li and Cheng, 1999). Using a modified freeze index model, Nan et al. (2012) predicted frozen ground distribution on the Tibetan Plateau over the next 50 to 100 years.

There are several methods to estimate soil freeze and thaw depths in cold regions: (1) using soil temperature data to estimate freeze-thaw depths (Frauenfeld et al., 2004; Zhang et al., 2005), (2) estimating the depths from the freeze-thaw index, and (3) using numerical models to estimate depths (Zhang and Stamnes, 1998). Of these, the annual freeze-thaw index is most widely used to determine the seasonal freeze and thaw depths in cold regions, primarily by using the Stefan equation (Nelson et al., 1997; Shiklomanov and Nelson, 2002; Zhang et al., 2005; Anisimov et al., 2007; Smith et al., 2009).

Many research papers have reported the surface and air freeze-thaw index by the daily soil ground surface and air temperature (Cheng et al., 2003; Wu and Liu, 2004; Jiang et al., 2007; Khalili et al., 2007; Wu et al., 2008; Zhao et al., 2008), but few regional-scale studies exist (Frauenfeld et al., 2007). Frauenfeld stated that the individual and combined interactions of soil temperature and freeze/thaw depth with changes in climatic variables at local, regional, and hemispheric scales are still poorly understood (Frauenfeld et al., 2004). Thus, in this paper, we document the regional-scale spatial and temporal variability of the freeze-thaw index and soil freezing depth over the Heihe River Basin in northwest China.

The goals of this research are as follows: to investigate changes in air and ground surface freezing/

thawing indices from 12 meteorological stations using in situ data and for the entire region using grid data and to evaluate the spatial and temporal variability of maximum freeze depths in the study area.

## DATA AND METHODS

### Study Area

This research was carried out in the Heihe River Basin, the second-largest inland river basin in northwest arid region of China ( $97^{\circ}42' E$ – $102^{\circ}04' E$  and  $37^{\circ}45' - 42^{\circ}40' N$ ;  $\sim 128,000 \text{ km}^2$ ) (Ma et al., 2002) (Fig. 1). The Heihe River flows northward through a piedmont diluvial-alluvial plain, an alluvial-lacustrine plain, and a desert. It also flows through three different climate zones: cold and humid or semiarid mountain zone, midstream temperate zone, and a downstream warm temperate zone (Zhang et al., 2003). Overall, climate in the Heihe River Basin is dry, with scarce, concentrated precipitation, strong winds, strong solar radiation, and large temperature differences between day and night (Lu et al., 2002; Pan and Li, 2011).

In field investigations, boreholes were drilled with depths ranging from 20 to 150 m and elevation spanning from 3600 m to 4132 m, then permafrost temperatures were measured about once a month after borehole drilling was completed. Permafrost temperatures were measured using a thermistor string with accuracy of  $0.05^{\circ}\text{C}$  in the laboratory calibration. Mean annual ground temperature varies from  $\sim 0$  to  $-1.5^{\circ}\text{C}$  with increasing elevation. The lower limit of permafrost distribution in the basin is at  $\sim 3650$  m a.s.l. (above sea level). Based on the lower limit, the result indicates that approximately  $14,100 \text{ km}^2$ , or 10.3%, of the Heihe River Basin consists of permafrost (Fig. 2) (Wang and Zhang, 2013).

### Data Collection

Data collected in this study include daily air temperature, daily ground surface temperature, and daily soil temperature at different depths; a digital elevation model (DEM); mean monthly grid air temperature; and land use data. The in situ temperature data were from China Meteorological Administration (CMA). Data from 24 meteorological stations (12 stations in the research region, and the other 12 stations nearby) were included (Table 1).

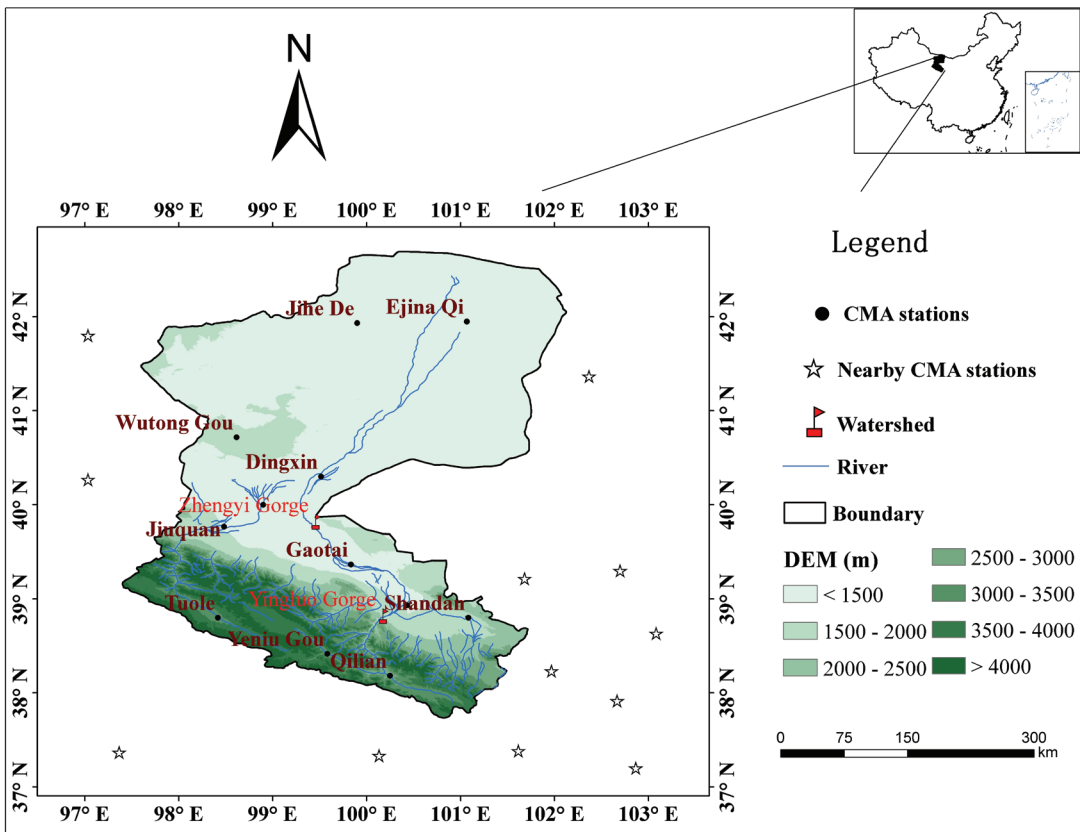


**FIGURE 1.** Geographic location of the Heihe River Basin in western China. CMA stations represent meteorological stations within the Heihe River Basin, while the nearby CMA stations are meteorological stations outside the Heihe River Basin.

The soil temperature data records (STT) ended in 2006, except Jihe De and Wutong Gou stations. The air and ground temperature records (AGTT) ended in 2013 also except Jihe De and Wutong Gou stations. The daily air temperature was used to estimate mean annual air temperature, air freezing/thawing index, and lapse rate. The daily ground surface temperature was used to calculate the surface freezing/thawing index, and the daily soil temperature was used to estimate the freeze depth in each station.

In addition, a 30-m-resolution DEM (Fig. 1) from the Environmental and Ecological Science Data Center for West China (<http://westdc.westgis.ac.cn/>) (Li et al., 2011), was used to adjust the monthly grid air temperature data for the complex terrain (from Fig. 1, we knew that the elevation varied from 500 m to more than 5000 m).

The mean monthly grid air temperatures on a 5-km-resolution grid from 2000 to 2009 was ac-

quired from the Environmental and Ecological Science Data Center for West China (<http://westdc.westgis.ac.cn/>) (Pan and Li, 2011). It was simulated by the Weather Research and Forecasting Model. Testing of the observational data revealed that the mean bias error of temperature was  $-0.19^{\circ}\text{C}$  and that the average correlation coefficient was 0.99 (Pan and Li, 2011). These data were used to calculate the air freezing/thawing index and freeze depth.

We obtained the land-use data from the GLC2000 project, which was coordinated by the Global Vegetation Monitoring Unit of the European Commission Joint Research Centre. This data set was derived from remote sensing platforms: the Advanced Very High Resolution Radiometer (AVHRR) (resolution 2.3–4.2 km) and the SPOT4 VGT sensor (vegetation; resolution 1.7 km). The Heihe River Basin is comprised of 11 types of land cover (Fig. 3) (Ran et al., 2010).

**TABLE 1**  
**Geographical information for meteorological stations in the Heihe River Basin, China.**

| Station    | Longitude (°E) | Latitude (°N) | Altitude (m a.s.l.) | STT       | AGTT      |
|------------|----------------|---------------|---------------------|-----------|-----------|
| Ejina Qi   | 101.07         | 41.95         | 940.5               | 1971~2006 | 1959~2013 |
| Jihe De    | 99.90          | 41.93         | 965.6               | 1971~1986 | 1958~1986 |
| Dingxin    | 99.52          | 40.30         | 1177.4              | 1957~2006 | 1955~2013 |
| Jinta      | 98.90          | 40.00         | 1270.5              | 1989~2006 | 1958~2013 |
| Gaotai     | 99.83          | 39.37         | 1332.2              | 1954~2006 | 1952~2013 |
| Jiuquan    | 98.48          | 39.77         | 1477.2              | 1959~2006 | 1951~2013 |
| Zhangye    | 100.43         | 38.93         | 1482.7              | 1959~2006 | 1951~2013 |
| Wutong Gou | 98.62          | 40.72         | 1591.0              | 1970~1988 | 1965~1988 |
| Shandan    | 101.08         | 38.80         | 1764.6              | 1955~2006 | 1952~2013 |
| Qilian     | 100.25         | 38.18         | 2787.4              | 1961~2006 | 1956~2013 |
| Yeniu Gou  | 99.58          | 38.42         | 3180.0              | 1980~2006 | 1959~2013 |
| Tuole      | 98.42          | 38.80         | 3367.0              | 1957~2006 | 1956~2013 |

STT is the soil temperature data time; AGTT is the air and ground surface temperature data time.

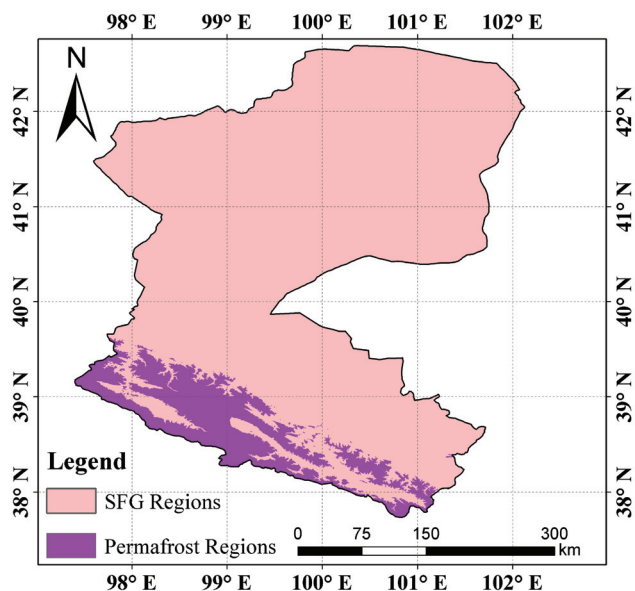


**FIGURE 2.** Map of frozen ground distribution in the Heihe River Basin in western China.

The land-use data were incorporated into the calculation of freeze depth (the method is listed in the Freezing Depth section).

## Methods

### Temperature Data

The daily soil temperature data were used to calculate the maximum soil freeze depth; there-

fore, we first considered the data from winter and spring because related research indicated that the maximum soil freeze depth occurred in winter and spring based on soil temperature data and field work in the area (Wang et al., 2013). There were several missing data situations, and we used the appropriate methods to make up for missing data. The first situation was that there were less than three missing data in one month. Here we used the mean soil temperature of the previous day and the following day to interpolate the daily soil temperature. The second situation was that there were more than three but less than five missing data in one month, in which case, we chose the nearest station (it was calculated by the distance and combined with higher coefficient  $R^2$ ) and used that data to build the linear dependence relation (it should be guaranteed the coefficient  $R^2$  is over 0.95 and the confidence level is 95%) and interpolated the missing data. The third situation was that there were more than five missing data in one month, in which case, we would delete the data for that year.

For the daily air temperatures and ground surface temperatures, we used the same method to make up for missing data. Based on the IPCC climatological baseline period from 1971 to 2000, we calculated the mean annual temperature departure with time period from 1960 to 2013.

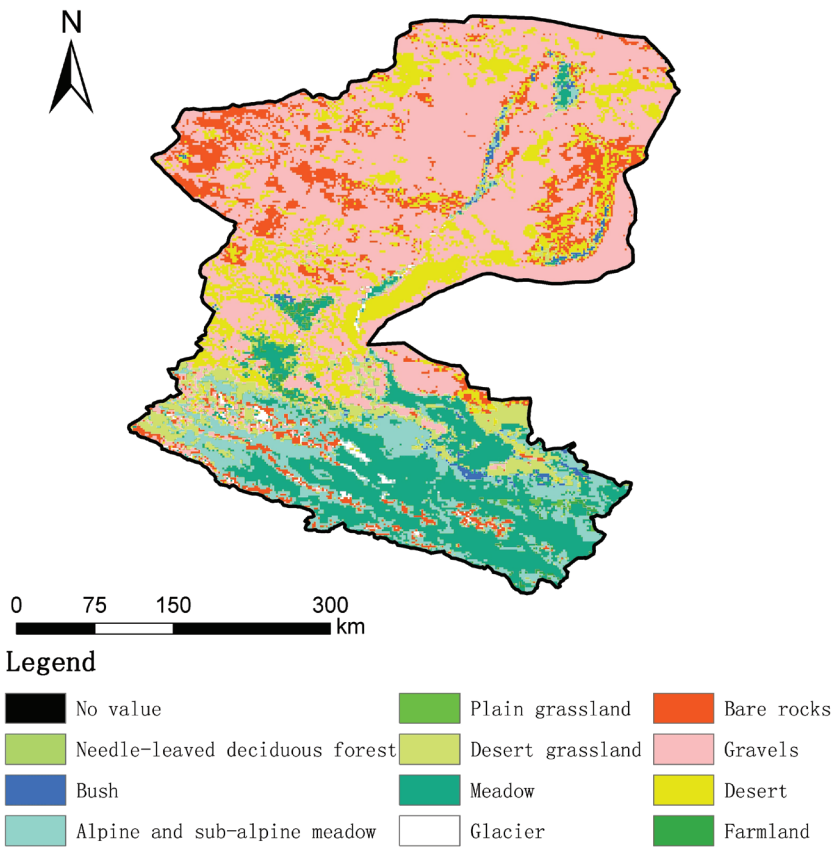


**FIGURE 3.** Land cover types of the Heihe River Basin in western China.

Based on the 5-km-resolution mean monthly grid air temperature, we obtained the 30-m grid temperature data using the topographical correction with the 30-m-resolution DEM. There were several steps, the first of which was to obtain the lapse rate. We used the mean monthly air temperature at the 12 meteorological stations in the Heihe River Basin to establish the relationship between mean monthly air temperature and elevation. Then, we determined the mean lapse rate (Table 2) for every month. Second, based on the 5-km mean monthly grid air temperature, we obtained grid latitude and longitude information, and the grid elevation value can be obtained using the DEM. Third, we set the 5-km mean monthly grid temperature down to sea level with the lapse rate. Fourth, we interpolated the grid data with ArcGIS software, using the Kriging method on the raster data. Fifth, using the lapse rate and 30 m DEM, we recalculated the mean monthly air temperature at the actual elevation with ArcGIS software. This way, we obtained the 30-m mean monthly grid air temperature over the study area. This method is widely

used, namely the topography adjustment method for the complicated terrain, especially mountainous areas (Willmott and Robeson, 1995).

**TABLE 2**  
The lapse rate of air temperature at 12 meteorological stations in the Heihe River Basin, China.

| Month | Lapse rate ( $^{\circ}\text{C } 100 \text{ m}^{-1}$ ) |
|-------|---|
| 1     | $-0.33 \pm 0.012$                                     |
| 2     | $-0.37 \pm 0.014$                                     |
| 3     | $-0.44 \pm 0.010$                                     |
| 4     | $-0.54 \pm 0.008$                                     |
| 5     | $-0.65 \pm 0.006$                                     |
| 6     | $-0.71 \pm 0.06$                                      |
| 7     | $-0.69 \pm 0.007$                                     |
| 8     | $-0.65 \pm 0.006$                                     |
| 9     | $-0.55 \pm 0.006$                                     |
| 10    | $-0.46 \pm 0.007$                                     |
| 11    | $-0.43 \pm 0.011$                                     |
| 12    | $-0.33 \pm 0.015$                                     |

## Annual Freezing/Thawing Index and the n Factor

We used mean daily air and ground surface temperatures at the meteorological stations to calculate the air and surface freezing and thawing indices ( $FI_a$ ,  $TI_a$ ,  $FI_s$ , and  $TI_s$ ) at the point scale and used the 30-m-grid temperature data to calculate the air freezing and thawing indices ( $FI_a$  and  $TI_a$ ) at the basin scale.

We calculated the annual air and surface freezing (thawing) index as the sum of the daily temperature for all days with temperatures below (above) 0 °C during the freezing (thawing) period. We defined the annual freezing period from 1 July through 30 June of the next year, and the thawing period from 1 January through 31 December (Steurer and Crandell, 1995; Zhang et al., 2005; Frauenfeld et al., 2007; Wu et al., 2011). The  $FI$  and  $TI$  could be estimated using the following:

$$FI = \sum_{i=1}^{N_F} |T_i| T_i < 0 \text{ } ^\circ\text{C} \quad (1)$$

$$TI = \sum_{i=1}^{N_T} T_i, T_i > 0 \text{ } ^\circ\text{C} \quad (2)$$

where  $N_F$  is the number of days with temperature below 0 °C;  $i = 1, 2 \dots N_F$ ;  $N_T$  is the number of days with temperatures above 0 °C; and  $T_i$  represents the temperature on a specific day.

Based on the freeze-thaw index, we calculated the  $n$  factor, which reflects the relationship between the air and surface freezing/thawing index:

$$n_f = \frac{FI_s}{FI_a} \quad n_t = \frac{TI_s}{TI_a} \quad (3)$$

## Trend Analysis

In this study, we used the parametric Unary Linear Regression Model, and moving average methods (three-point moving average) to analyze trends (Xu, 2002; Stow et al., 2003).

## Freezing Depth

There were many methods to estimate soil freezing depth, such as soil temperature measurements, numerical models, and the Stefan formula. We used the Stefan formula to estimate soil freezing depth:

$$MFP = \sqrt{2k_f \left( \frac{n_f DDFa}{P_b w L} \right)} \quad (4)$$

where  $MFP$  is frozen depth (m),  $K_f$  represents the thermal conductivity of frozen soils ( $\text{W m}^{-1} \text{ } ^\circ\text{C}^{-1}$ ),  $n_f$  is  $n$  factor for the freezing season,  $DDFa$  is the annual air freezing index ( $^\circ\text{C d}$ ),  $P_b$  is the soil bulk density ( $\text{kg m}^{-3}$ ),  $w$  is the soil water content by weight, and  $L$  is the latent heat of fusion ( $\text{J kg}^{-1}$ ) (Zhang et al., 2005). From this, we can see that there are many factors in estimating soil freezing depth and that it was difficult to obtain these data sets for large regions. Figure 4 indicates the relationship between  $DDFa$  and  $MFP$ , the linear relation correlated well by slope at 0.11, with an  $R^2$  greater than 0.5 and statistical significances as high as  $p < 0.05$ . Thus, we can simplify Equation 4 to Equation 5 (Harlan and Nixon, 1978):

$$MFP = E \sqrt{DDFa} \quad (5)$$

where  $E$  was defined in Equation 6 (Nelson and Outcalt, 1987):

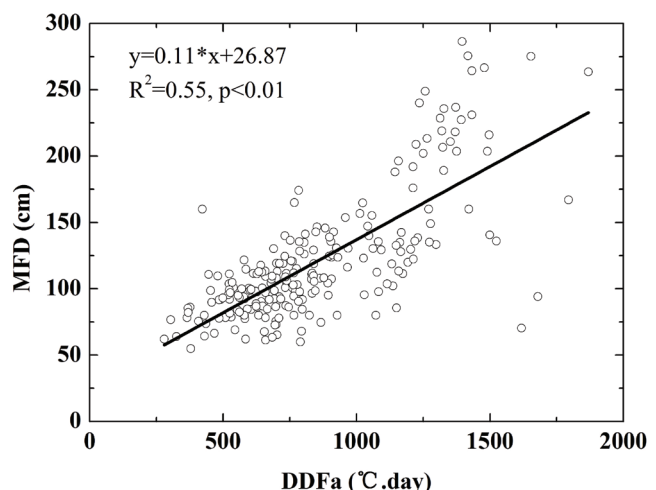


**FIGURE 4.** Linear relationship between the maximum freeze depth and the annual freezing index of air temperature (DDFa). Data used are from all meteorological stations within and outside the Heihe River Basin in western China as shown in Figure 1.

$$E = \sqrt{\frac{2k_f n_f}{P_b w l}} \quad (6)$$

To obtain  $E$ , we used soil temperature data from the 12 meteorological stations in the Heihe River Basin and 12 other stations near the river basin. We interpolated the depth of the 0 °C isotherm throughout the 0.0–3.2 m soil temperature profiles by linear method (Frauenfeld et al., 2004). Therefore, we estimated  $E$  value base on *MFP* and *DDFa* at every station using Equation 6. Past research has indicated that the  $E$  factor was mainly affected by land use (Zhang et al., 2005).

Thus, based on land use type from the 24 stations, the  $E$  value can be divided into 11 groups. For each group, we obtain an average  $E$  value as summarized in Table 3. Table 3 represents the mean and standard deviation of  $E$  with different land cover types. The average  $E$  value varied from 0.028 to 0.053. The gravels were highest at 0.053, followed by bare rocks at 0.049. The minimum was desert at 0.028. The standard deviation of alpine and subalpine meadow was the largest at 0.023. The smallest was for plain grassland at 0.003 and bare rocks at 0.004. Because there were no stations with land cover types of needle-leaved deciduous forest in the study area, no  $E$  value was obtained, thus we could not estimate the freeze depth for regions with needle-leaved deciduous forest.

**TABLE 3**  
**Mean values of E and their standard deviation across different land cover types in the Heihe River Basin, China.**

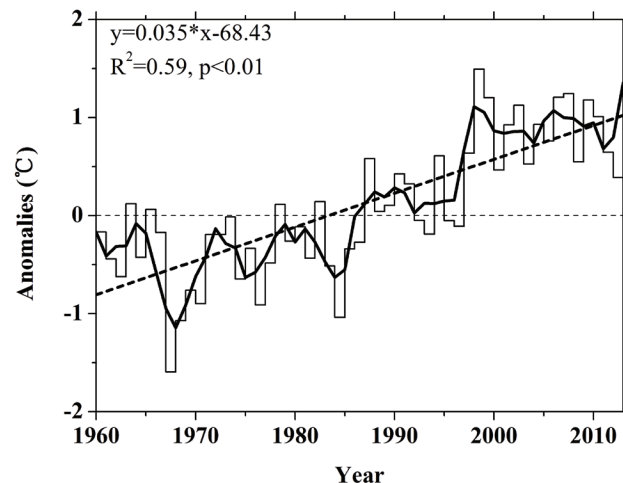
| Land cover type                | Mean E   | Std. dev. |
|--------------------------------|----------|-----------|
| Bush                           | 0.042    | 0.006     |
| Alpine and subalpine meadow    | 0.034    | 0.023     |
| Plains grassland               | 0.037    | 0.003     |
| Desert grassland               | 0.032    | 0.008     |
| Meadow                         | 0.041    | 0.011     |
| Bare rocks                     | 0.049    | 0.004     |
| Gravels                        | 0.053    | 0.005     |
| Desert                         | 0.028    | 0.011     |
| Farmland                       | 0.045    | 0.008     |
| Needle-leaved deciduous forest | No value | No value  |
| Glacier                        | No value | No value  |

## RESULTS

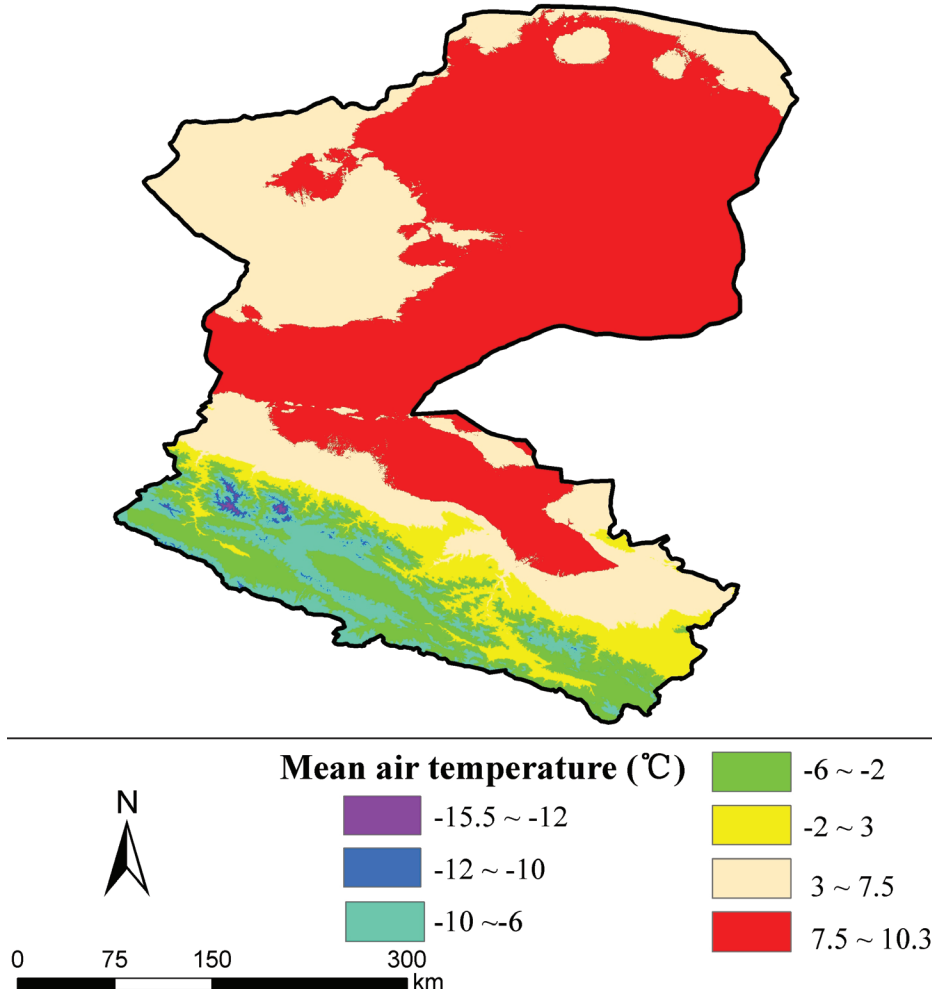
### Air Temperature Change

Figure 5 represents the variation trend of mean annual air temperature anomaly from 1960 to 2013 for the 12 sites with daily air temperature observations. The trend exhibited a statistically significant ( $p < 0.01$ ) increase over the 1960–2013 period of 0.35 °C decade $^{-1}$ , or approximate change of 1.9 °C for the 54-year period. From late 1987 onward, air temperature has been above the long-term (1971–2000) average. In addition to this long-term increase, the time series also indicated some large interdecadal variability. Mean annual air temperature increased slightly from 1962 to 1965, and this was followed by a sharp decrease until 1970. From 1970 to 1998, however, mean annual air temperature increased dramatically. After 1998, a slight decrease occurred. The overall 1960–2013 change was therefore largely driven by the increase during the 1970–1998 periods.

Based on monthly grid air temperature from 2000 to 2009, the spatial variation of mean annual air temperature (Fig. 6) showed that mean annual air temperature of less than –2 °C appeared in the upper reaches of Heihe River Basin. The highest temperature, ranging from 7.5 to 10.3 °C, occurred in the mid- and downstream regions with low altitude and sparse vegetation. The overall spatial varia-



**FIGURE 5.** Anomalies of mean annual air temperature from its long-term (1971–2000) mean in the Heihe River Basin from 1960 to 2013. The thick black dashed line is the linear trend during the study period. The thick black line is the smoothing average.



**FIGURE 6.** The mean annual air temperature from 2000 to 2009 in the Heihe River Basin.

tion of mean annual air temperature was that it was colder in the south and warmer in the north.

### Changes in Freezing/Thawing Indices

Of the total 12 stations with daily air and surface temperature, the  $FI_a$ ,  $FI_s$ ,  $TI_a$ , and  $TI_s$  were estimated. Linear trend and moving average methods were used to analyze their variability (Figs. 7 and 8).

Figure 7 presents a time series of  $FI_a$  and  $FI_s$ . They clearly exhibited decreasing trends over the period of the station data with  $p < 0.05$ . The trend of  $FI_a$  in Shandan station, and trend of  $FI_s$  in Ejina Qi station were slightly larger than other stations, with statistical significances  $p < 0.05$ .  $FI_a$  and  $FI_s$  varied between  $300 \text{ }^{\circ}\text{C d}$  and  $2400 \text{ }^{\circ}\text{C d}$  during the period. In general,  $FI_s$  was smaller than  $FI_a$  in the same period, indicating winter ground surface temperature is higher than air temperature. Furthermore, the difference between  $FI_a$  and  $FI_s$  was

larger with altitude increase. The probable reason was that the differences between air temperature and ground surface temperature were larger in the high altitude regions.  $FI_a$  and  $FI_s$  increase with elevation, indicating winter air temperature decreases with elevation increase.

Figure 8 indicated the linear trends of the thawing index, including  $TI_a$  and  $TI_s$  for observational stations. It clearly exhibited increasing trends over the period of the station data with  $p < 0.05$ . The resulting changes in  $TI_a$  and  $TI_s$  ranged between  $886$  and  $4641 \text{ }^{\circ}\text{C d}$ , and between  $1664$  and  $6036 \text{ }^{\circ}\text{C d}$ , respectively. The fastest increase of  $TI_a$  was by Ejina Qi station at  $9.70 \text{ }^{\circ}\text{C d yr}^{-1}$ , and followed by Zhangye station at  $8.44 \text{ }^{\circ}\text{C d yr}^{-1}$ . The slowest increase of  $TI_a$  was by Gaotai station at  $4.52 \text{ }^{\circ}\text{C d yr}^{-1}$ . For  $TI_s$ , the fastest increase was also by Ejina Qi at  $15.76 \text{ }^{\circ}\text{C d yr}^{-1}$ , followed by Zhangye at  $13.12 \text{ }^{\circ}\text{C d yr}^{-1}$ , respectively. However, the slowest increase was by Tuole station at  $3.75 \text{ }^{\circ}\text{C d yr}^{-1}$ .

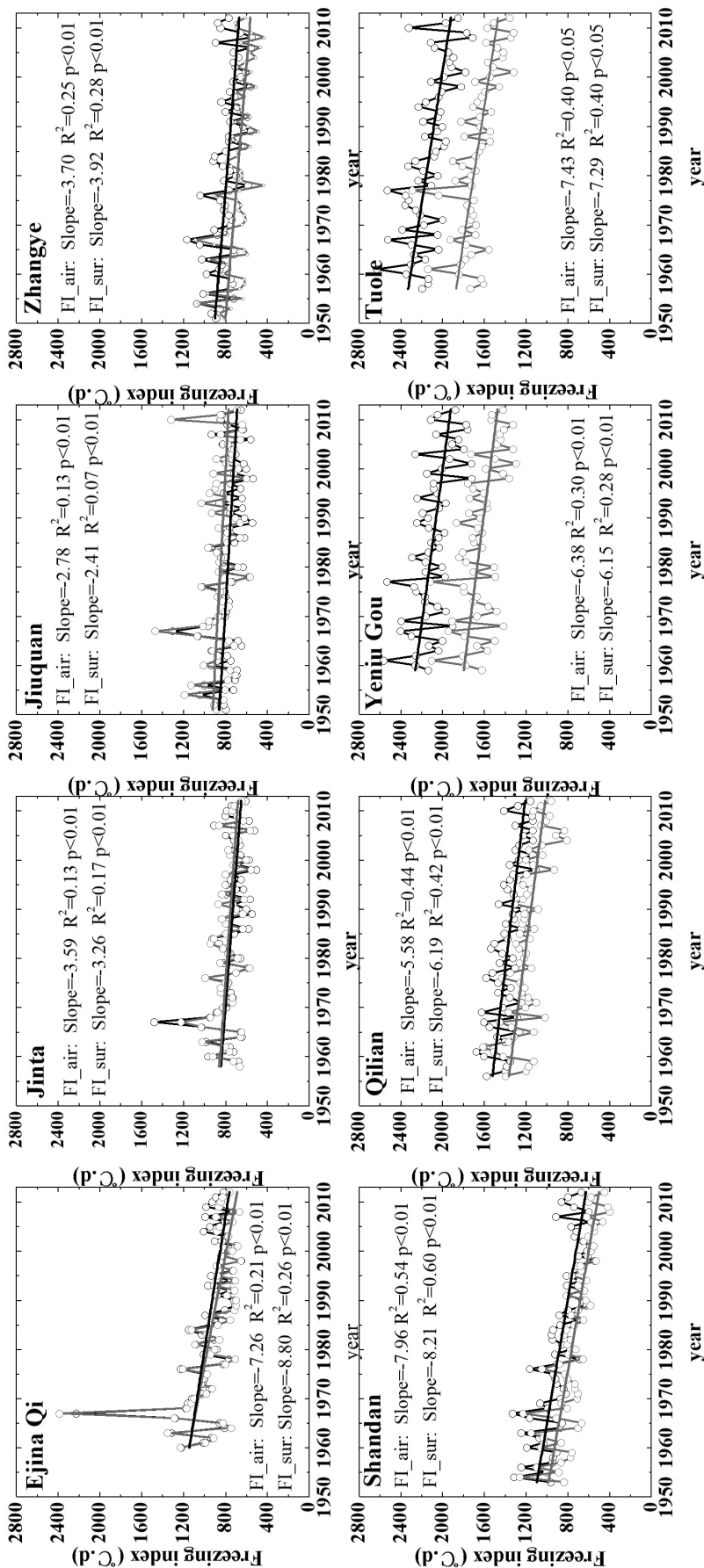


FIGURE 7. Linear trends of freezing index for 8 meteorological stations within the Heihe River Basin. The thick black line is the linear trend of air freezing index, and the gray line is the trend of ground surface freezing index.

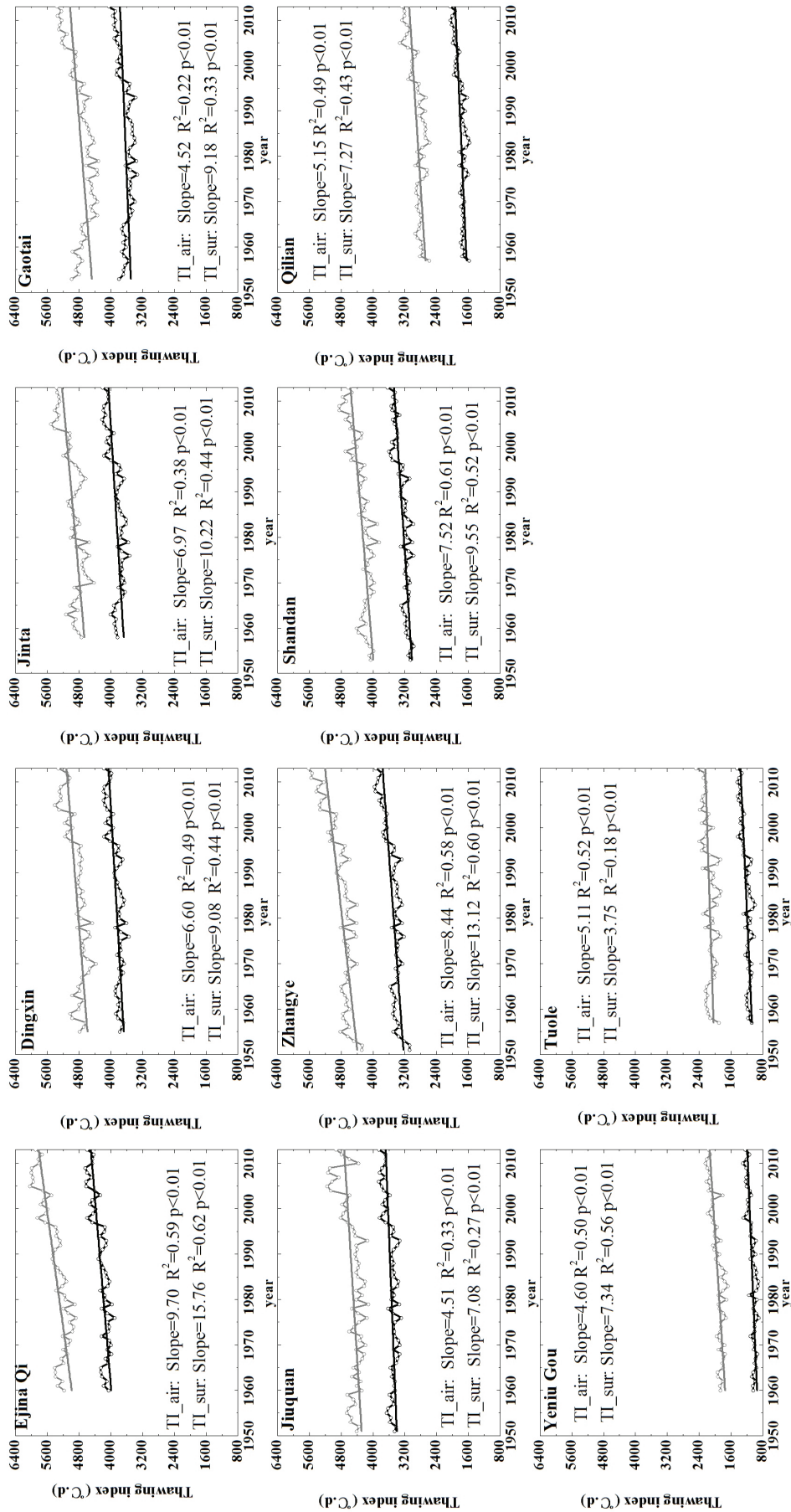
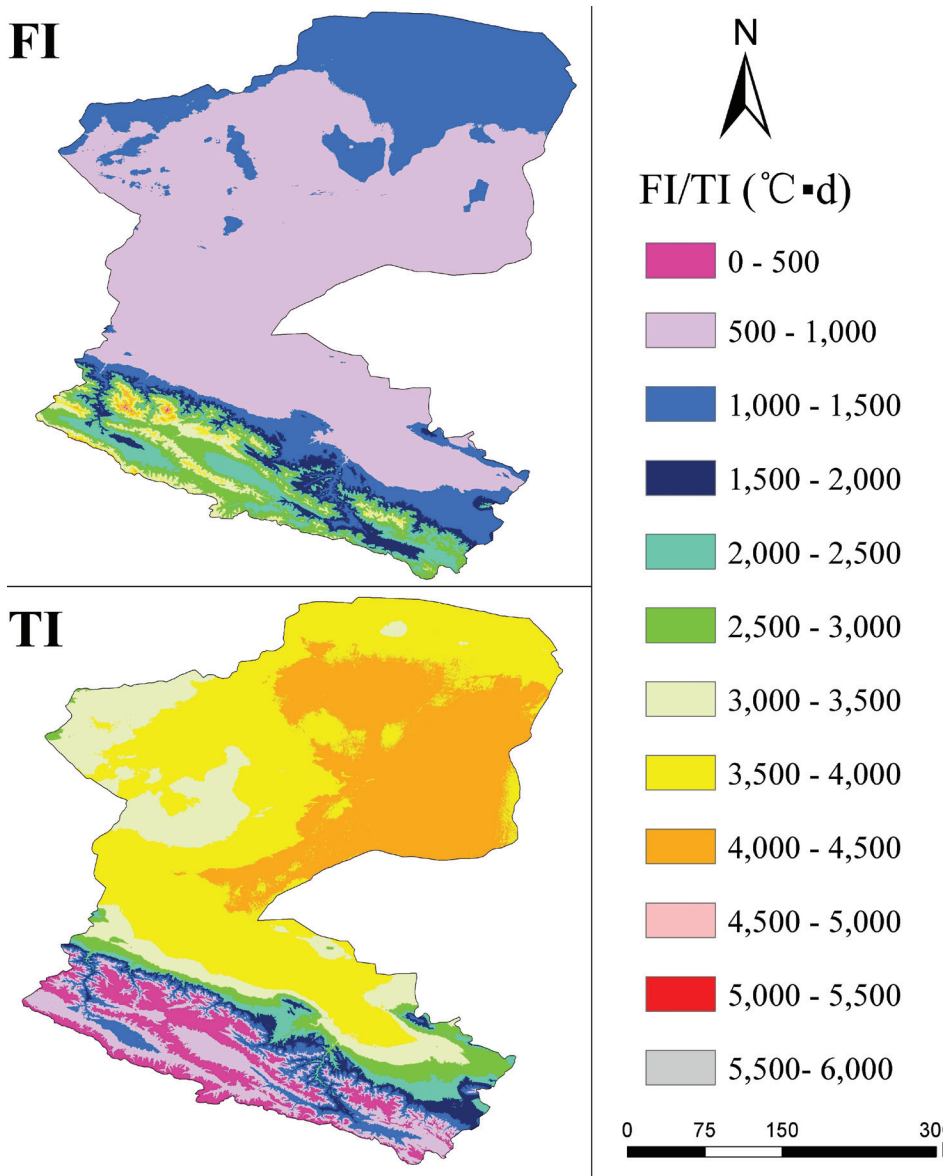


FIGURE 8. Linear trends of thawing index for 10 meteorological stations within the Heihe River Basin. The thick black line is the linear trend of air thawing index, and the gray line is the trend of ground surface thawing index.



**FIGURE 9.** Spatial variation of annual air freezing index (FI) and thawing index (TI) in the Heihe River Basin, China.

Except for  $FI_a$  and  $TI_a$  at the point scale, we also used the 30-m grid mean monthly air temperature to calculate the  $FI_a$  and  $TI_a$  from 2000 to 2008 (Fig. 9). The time series trend of  $FI_a$  and  $TI_a$  were also estimated by the linear trend method, but with statistical significances as high as  $p > 0.1$ . Thus, the variation trends are not discussed in this paper.

Figure 9 exhibits the distribution of  $FI_a$  ranging from 624–5646 °C d. Spatially,  $FI_a$  in the lower and middle reaches of Heihe River Basin was less than 1000 °C d, and in the upper reaches, it was 1000–5600 °C d.  $FI_a$  in the eastern part of the river basin was larger than in the west. Figure 9 shows that  $TI_a$  varied from 0 to 4558 °C d from 2000 to 2009.  $TI_a$  was greater than 3000 °C d in the downstream and midstream regions, and in the upstream

region it was less than 3000 °C d.  $TI_a$  was larger in the north and east, and smaller in the south and west. In general, the spatial distribution of  $TI_a$  was opposite to  $FI_a$ .

#### $n_f$ and $n_t$

To compare with  $FI$  and  $TI$  at 12 observation stations,  $n_f$  and  $n_t$  were introduced in this paper. Table 4 presents the character of these parameters. The  $n_f$  ranged from 0.78 to 1.09. Jiuquan station ranked first at 1.09, and the last was Yeniu Gou station at 0.78. As for  $n_t$ , the range was between 1.26 and 1.82. Yeniu Gou station ranked first, followed by Tuole station, while  $n_t$  was lowest at Ejina Qi and Dingxin stations. The mean  $n_f$  was less than 1.0, and

TABLE 4

$n_f$  and  $n_t$  at the 12 meteorological stations in the Heihe River Basin, China.

| Station    | $n_f$ | $n_t$ |
|------------|-------|-------|
| Ejina Qi   | 0.96  | 1.27  |
| Jihe De    | 0.84  | 1.28  |
| Dingxin    | 0.99  | 1.26  |
| Jinta      | 1.03  | 1.28  |
| Gaotai     | 0.94  | 1.31  |
| Jiuquan    | 1.09  | 1.27  |
| Zhangye    | 0.87  | 1.37  |
| Wutong Gou | 0.90  | 1.32  |
| Shandan    | 0.86  | 1.32  |
| Qilian     | 0.87  | 1.61  |
| Yeniu Gou  | 0.78  | 1.82  |
| Tuole      | 0.79  | 1.77  |
| Mean       | 0.91  | 1.41  |

the  $n_t$  was more than 1.0. It can be clearly seen that  $n_t$  was larger than  $n_f$ .

These results indicated that the  $FI$  was less than  $TI$ . Furthermore, the change of these parameters correlated with elevation. Thus, we estimated the relationship between  $FI$ ,  $TI$ , these parameters, and elevation (Table 5). It was clear that  $FI$  and  $n_t$  were positively correlated with elevation with statistical significances as high as  $p < 0.05$ . This means that these two parameters increased as elevation increased. However,  $TI$  and  $n_f$  were negatively correlated with elevation. The reason was that elevation affected the air temperature more

than the ground surface temperature, because air temperature was controlled by the atmospheric state and related with air pressure. However, the ground surface temperature was controlled by the surface energy balance, and had no direct relation with elevation. Thus, the changes in ground surface temperature may be slower (Zhao et al., 2008).

## Spatial and Temporal Variability of the Freezing Depth

Using the air freezing index and  $E$  values, we estimated the soil freezing depth over the period 2000 to 2008. In the permafrost regions, the freezing depth was the potential seasonal freezing depth, while in SFG, the freezing depth was the maximum freezing depth.

Table 6 and 7 show the total area and area fraction of the maximum freezing depth from 2000 to 2008 with six ranges of <1 m, 1–1.5 m, 1.5–2.5 m, 2.5–3.5 m, >3.5 m, and no value. With freezing depths of <1 m and 1–1.5 m, the maximum and the minimum area occurred in 2008 and 2004, respectively. The maximum area was  $3.221 \times 10^4 \text{ km}^2$  or 28.2% of the SFG region in 2008, and  $7.584 \times 10^4 \text{ km}^2$  or 66.4% in 2004. The minimum area was 0 and  $2.655 \times 10^4 \text{ km}^2$ , respectively. On the other hand, with freezing depth ranges of 1.5–2.5 m and 2.5–3.5 m, the areas ranking first and last occurred in 2004 and 2008, respectively. Overall, it was approximately 58.1% and 0.04% of SFG regions where soil maximum freeze depth ranged between 1.5 m and 2.5 m, and between 2.5 m and 3.5 m, respectively. Meanwhile, approximately  $0.0302 \times 10^4 \text{ km}^2$  at 0.26% of the SFG region area had no value.

Tables 8 and 9 indicate the potential seasonal freezing depth in the permafrost region from 2000 to 2008. It is clear that there was no place with a potential seasonal freezing depth less than 1 m in this region. Meanwhile, with a potential seasonal freezing depth range of 1–1.5, 2.5–3.5, and >3.5 m, the largest area was less than  $0.20 \times 10^4$ ,  $0.360 \times 10^4$ , and  $0.0020 \times 10^4 \text{ km}^2$ , respectively. Additionally, the percentage of area covered by these three ranges was less than 26%. Meanwhile, the area with a potential seasonal freezing depth range of 1.5–2.5 m was more than  $0.935 \times 10^4 \text{ km}^2$ , and the percentage more than 67.9%. There were also some

TABLE 5

Linear relationship between factors and elevation.

| Parameters | Slope    | $R^2$ | $P$    |
|------------|----------|-------|--------|
| FIa        | 0.55     | 0.83  | 0.00** |
| FIs        | 0.38     | 0.82  | 0.00** |
| TIa        | -1.30    | 0.99  | 0.00** |
| TIs        | -1.38    | 0.98  | 0.00** |
| $n_f$      | -0.00007 | 0.41  | 0.03*  |
| $n_t$      | 0.0002   | 0.93  | 0.00** |

Note: the symbol \*\* indicates that the statistical significances is as high as  $p < 0.01$ ; while symbol \* indicates that the statistical significances is as high as  $p < 0.05$ .

permafrost places with no value at  $0.0655 \times 10^4$  km<sup>2</sup> or 4.8% of this study region.

Figure 10 shows the mean freezing depth in the Heihe River Basin. The region in which the freezing depth was <1 m was mainly in the midstream portion of the basin and in a part of the downstream portion. The region with freezing depth between 1 and 1.5 m occupied most of the midstream region, between 1.5 and 2.5 m was in the upstream and downstream regions, while the freezing depth was deeper than 2.5 m in the entire upstream region.

It can be clearly seen that a potential seasonal freezing depth of 1.5–2.5 m was observed in most of the permafrost regions, and maximum freezing depth below 2.5 m was in most of the SFG regions.

## SUMMARY AND CONCLUSIONS

This paper conducted a detailed investigation of changes in air temperature, freezing/thawing indices, and soil freeze depths in Heihe River Basin.

The mean annual air temperature had a significant increase at the rate of 0.35 °C decade<sup>-1</sup> from 1960 to 2013, for a total increase of 1.9 °C for the 54-year period. For the spatial variation of mean annual air temperature, it was colder in the south at higher elevations and warmer in the north at lower elevations.

As for the  $FI_a$  and  $TI_a$  at site scale, we found that the  $FI_a$  and  $FI_s$  varied between 300 °C d and 2400 °C d during the observation period. A decreasing trend was obvious over the period of the station data, with  $p < 0.05$ . Changes in  $TI_a$  and  $TI_s$  ranged between 886 °C d and 4641 °C d, and between 1664 °C d and 6036 °C d, respectively. Meanwhile, the increasing trend was significant during the observation period. At the regional scale,  $FI_a$  and  $TI_a$  varied from 624 to 5646 °C d and from 0 to 4558 °C d, respectively.

The parameters including  $n_f$  and  $n_t$  at 12 meteorological stations in the study area revealed that  $n_t$  was more than 1.0 and  $n_f$  less than 1.0. Meanwhile,

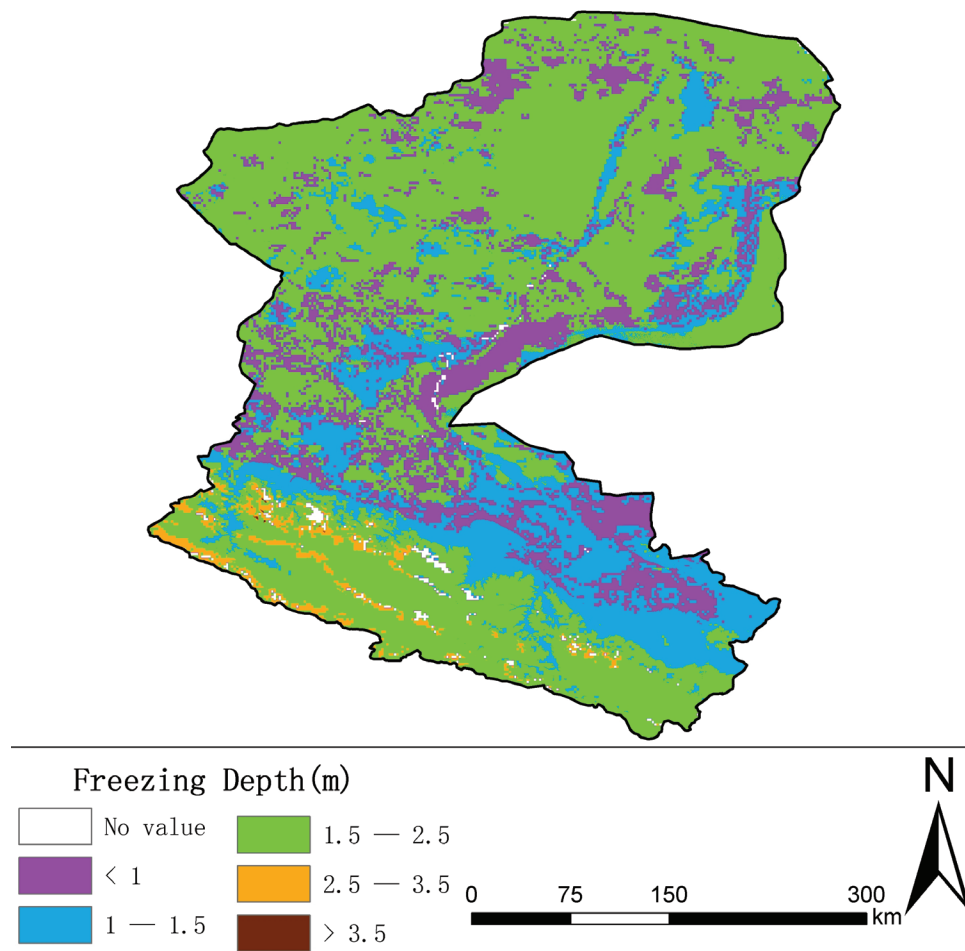


FIGURE 10. The mean freezing depth from 2000 to 2008 in the Heihe River Basin, China.

**TABLE 6**  
**Maximum freezing depths in the seasonally frozen ground area from 2000 to 2008.**

| Freezing depth (m) | Area ( $\times 10^4 \text{ km}^2$ ) |       |       |       |       |        |        |       |        |           |
|--------------------|-------------------------------------|-------|-------|-------|-------|--------|--------|-------|--------|-----------|
|                    | 2000                                | 2001  | 2002  | 2003  | 2004  | 2005   | 2006   | 2007  | 2008   | 2000~2008 |
| < 1                | 2.917                               | 2.762 | 2.139 | 2.127 | 0.0   | 2.104  | 3.111  | 2.263 | 3.221  | 2.242     |
| 1~1.5              | 5.701                               | 4.154 | 2.246 | 2.316 | 2.655 | 3.471  | 7.384  | 2.214 | 7.584  | 2.513     |
| 1.5~2.5            | 2.773                               | 4.479 | 7.0   | 6.936 | 8.703 | 5.821  | 0.901  | 6.916 | 0.592  | 6.635     |
| 2.5~3.5            | 0.002                               | 0.001 | 0.012 | 0.018 | 0.039 | 0.0023 | 0.0005 | 0.003 | 0.0002 | 0.004     |
| >3.5               | 0.0                                 | 0.0   | 0.0   | 0.0   | 0.0   | 0.0    | 0.0    | 0.0   | 0.0    | 0.0       |
| No value           | 0.0302                              |       |       |       |       |        |        |       |        |           |

**TABLE 7**  
**Areal percentage of maximum freezing depths in the seasonally frozen ground area from 2000 to 2008.**

| Frozen depth (m) | Percentage (%) |      |      |      |      |      |       |      |       |           |
|------------------|----------------|------|------|------|------|------|-------|------|-------|-----------|
|                  | 2000           | 2001 | 2002 | 2003 | 2004 | 2005 | 2006  | 2007 | 2008  | 2000~2008 |
| <1               | 25.5           | 24.2 | 18.7 | 18.6 | 0.0  | 18.4 | 27.2  | 19.8 | 28.2  | 19.6      |
| 1~1.5            | 49.9           | 36.4 | 19.7 | 20.3 | 23.2 | 30.4 | 64.6  | 19.4 | 66.4  | 22.0      |
| 1.5~2.5          | 24.3           | 39.2 | 61.3 | 60.7 | 76.2 | 50.9 | 7.9   | 60.5 | 5.2   | 58.1      |
| 2.5~3.5          | 0.02           | 0.01 | 0.11 | 0.16 | 0.35 | 0.02 | 0.005 | 0.03 | 0.002 | 0.04      |
| >3.5             | 0.0            | 0.0  | 0.0  | 0.0  | 0.0  | 0.0  | 0.0   | 0.0  | 0.0   | 0.0       |
| No value         |                |      |      |      | 0.26 |      |       |      |       |           |

**TABLE 8**  
**Potential seasonal freezing depth in the permafrost area from 2000 to 2008.**

| Freezing depth (m) | Area ( $\times 10^4 \text{ km}^2$ ) |        |        |       |        |        |        |        |        |           |
|--------------------|-------------------------------------|--------|--------|-------|--------|--------|--------|--------|--------|-----------|
|                    | 2000                                | 2001   | 2002   | 2003  | 2004   | 2005   | 2006   | 2007   | 2008   | 2000~2008 |
| <1                 | 0.0                                 | 0.0    | 0.0    | 0.0   | 0.0    | 0.0    | 0.0    | 0.0    | 0.0    | 0.0       |
| 1~1.5              | 0.021                               | 0.051  | 0.004  | 0.002 | 0.0003 | 0.021  | 0.099  | 0.019  | 0.16   | 0.008     |
| 1.5~2.5            | 1.061                               | 1.059  | 1.025  | 0.985 | 0.935  | 1.087  | 1.061  | 1.076  | 1.031  | 1.059     |
| 2.5~3.5            | 0.228                               | 0.201  | 0.279  | 0.314 | 0.357  | 0.203  | 0.151  | 0.216  | 0.120  | 0.244     |
| >3.5               | 0.0019                              | 0.0012 | 0.0046 | 0.011 | 0.019  | 0.0002 | 0.0002 | 0.0012 | 0.0003 | 0.0017    |
| No value           |                                     |        |        |       | 0.0655 |        |        |        |        |           |

**TABLE 9**  
**Areal percentage of potential seasonal freezing depth in the permafrost area from 2000 to 2008.**

| Frozen depth (m) | Percentage (%) |      |      |      |       |      |      |      |      |           |
|------------------|----------------|------|------|------|-------|------|------|------|------|-----------|
|                  | 2000           | 2001 | 2002 | 2003 | 2004  | 2005 | 2006 | 2007 | 2008 | 2000~2008 |
| <1               | 0.0            | 0.0  | 0.0  | 0.0  | 0.0   | 0.0  | 0.0  | 0.0  | 0.0  | 0.0       |
| 1~1.5            | 1.6            | 3.7  | 3.0  | 0.2  | 0.002 | 1.6  | 7.3  | 1.4  | 11.7 | 0.6       |
| 1.5~2.5          | 77.0           | 76.8 | 74.4 | 71.5 | 67.9  | 78.9 | 77.0 | 78.1 | 74.8 | 76.8      |
| 2.5~3.5          | 16.5           | 14.6 | 20.2 | 22.8 | 25.9  | 14.8 | 11.0 | 15.7 | 8.7  | 17.7      |
| >3.5             | 0.1            | 0.1  | 0.3  | 0.8  | 1.4   | 0.01 | 0.02 | 0.1  | 0.02 | 0.1       |
| No value         |                |      |      |      | 4.8   |      |      |      |      |           |

the negative relation between  $TI$ ,  $n_p$ , and elevation was significant, while a positive relation was seen with other parameters.

Combining the  $E$  values across the study area with the freezing index, we obtained the distribution of freezing depth in the Heihe River Basin. The freezing depth was deeper than 1 m in most of the study area. In the midstream region, the freeze depth was 1–1.5 m; in the downstream area it was 1.5–2.5 m, and in the upstream freeze depth was >1.5 m (and usually deeper than 2 m). The potential seasonal freezing depth was 1.5–2.5 m in most of the permafrost regions of the study area. However, most of the SFG regions had a maximum freezing depth below 2.5 m within the study area.

## ACKNOWLEDGMENTS

This study was supported by the Natural Science Foundation of China (grant 91325202), the National Key Scientific Research Program of China (grant 2013CBA01802), and the Fundamental Research Funds for the Central Universities (grant lzujbky-2015-217). We appreciate the thoughtful suggestions and comments from two anonymous reviewers, whose comments help to improve the manuscript. The 5-km-grid air temperature, 30-m DEM, and land cover data were obtained from the Environmental and Ecological Science Data Center for West China (<http://westdc.westgis.ac.cn/>). We acknowledge computing resources and time at the Supercomputing Center of Cold and Arid Region Environment and Engineering Research Institute of Chinese Academy of Sciences

## REFERENCES CITED

- Anisimov, O. A., Lobanov, V. A., Reneva, S. A., Shiklomanov, N. I., Zhang, T., and Nelson, F. E., 2007: Uncertainties in gridded air temperature fields and effects on predictive active layer modeling. *Journal of Geophysical Research: Earth Surface* (2003–2012), 112(F2): doi <http://dx.doi.org/10.1029/2006JF000593>.
- Cheng, G. D., and Xu, X. Z., 1993: Research progress of Chinese geocryology viewed from 6th International Conference on Permafrost. *Journal of Glaciology and Geocryology*, 15(3): 421–423.
- Cheng, G. D., Jiang, H., Wang, K. L., and Wu, Q. B., 2003: Thawing index and freezing index on the embankment surface in permafrost regions. *Journal of Glaciology and Geocryology*, 25(6): 603–607.
- Frauenfeld, O. W., Zhang, T., Barry, R. G., and Gilichinsky, D., 2004: Interdecadal changes in seasonal freeze and thaw depths in Russia. *Journal of Geophysical Research: Atmospheres* (1984–2012), 109(D5): doi <http://dx.doi.org/10.1029/2003JD004245>.
- Frauenfeld, O. W., Zhang, T., and McCreight, J. L., 2007: Northern hemisphere freezing/thawing index variations over the twentieth century. *International Journal of Climatology*, 27(1): 47–63.
- Harlan, R., and Nixon, J., 1978: Ground thermal regime. *Geotechnical Engineering for Cold Regions*: 103–163.
- Jiang, F., Hu, R., and Li, Z., 2007: Variation trends of the freezing and thawing index along the Qinghai-Xizang Railway for the period 1966–2004. *Acta Geographica Sinica-Chinese Edition*, 62(9): 935.
- Jingkang, D., and Guisheng, H., 2000: The critical value of mean annual air temperature an important factor for designing the critical height of embankment in permafrost regions of the Tibetan Plateau. *Journal of Glaciology and Geocryology*, 22(4): 333–339.
- Khalili, A., Rahimi, H., and Shariatmadari, Z. A., 2007: Validation of air freezing index (AFI), for determination of frost penetration depth in typical arid and semi-arid zones of Iran. *Desert*, 12(1): 23–31.
- Li, S.-x., and Wu, T.-h., 2004: Permafrost temperature regime: study method and applied analysis. *Journal of Glaciology and Geocryology*, 26(4): 377–383.
- Li, X., and Cheng, G., 1999: A GIS-aided response model of high-altitude permafrost to global change. *Science in China Series D: Earth Sciences*, 42(1): 72–79.
- Li, X., Nan, Z., Cheng, G., Ding, Y., Wu, L., Wang, L., Wang, J., Ran, Y., Li, H., and Pan, X., 2011: Toward an improved data stewardship and service for environmental and ecological science data in West China. *International Journal of Digital Earth*, 4(4): 347–359.
- Lu, L., Li, X., and Cheng, G.-D., 2002: Analysis on the seasonal phenological characteristics of the Heihe River Basin with AVHRR NDVI data set. In Proceedings, Geoscience and Remote Sensing Symposium, IEEE International, 1997–1999.
- Lunardini, V., 1996: Climatic warming and the degradation of warm permafrost. *Permafrost and Periglacial Processes*, 7(4): 311–320.
- Ma, M.-G., Jiao, Y.-M., Wang, X.-M., and Cheng, G.-D., 2002: The TM/ETM+ Mosaic image processing and application in the Heihe River Basin. *Journal of Glaciology and Geocryology*, 24(4): 451–456.
- Nan, Z., Li, S., Cheng, G., and Huang, P., 2012: Surface frost number model and its application to the Tibetan plateau. *Journal of Glaciology and Geocryology*, 34(1): 89–95.
- Nelson, F. E., 2003: (Un) frozen in time. *Science*, 299(5613): 1673–1675.
- Nelson, F. E., and Outcalt, S. I., 1987: A computational method for prediction and regionalization of permafrost. *Arctic and Alpine Research*, 279–288.
- Nelson, F., Shiklomanov, N., Mueller, G., Hinkel, K., Walker, D., and Bockheim, J., 1997: Estimating active-layer thickness

- over a large region: Kuparuk River basin, Alaska, USA. *Arctic and Alpine Research*: 367–378.
- Pan, X. D., and Li, X., 2011: Validation of WRF model on simulating forcing data for Heihe River Basin. *Science in Cold and Arid Regions*, 3(4).
- Ran, Y., Li, X., and Lu, L., 2010: Evaluation of four remote sensing based land cover products over China. *International Journal of Remote Sensing*, 31(2): 391–401.
- Shiklomanov, N. I., 2012: Non-climatic factors and long-term, continental-scale changes in seasonally frozen ground. *Environmental Research Letters*, 7(1): 011003, doi <http://dx.doi.org/10.1088/1748-9326/7/1/011003>.
- Shiklomanov, N., and Nelson, F., 2002: Active-layer mapping at regional scales: a 13-year spatial time series for the Kuparuk region, north-central Alaska. *Permafrost and Periglacial Processes*, 13(3): 219–230.
- Smith, S. L., Wolfe, S. A., Riseborough, D. W., and Nixon, F. M., 2009: Active-layer characteristics and summer climatic indices, Mackenzie Valley, Northwest Territories, Canada. *Permafrost and Periglacial Processes*, 20(2): 201–220.
- Steurer, P. M., 1996: Probability distributions used in 100-year return period of air-freezing index. *Journal of Cold Regions Engineering*, 10(1): 25–35.
- Steurer, P. M., and Crandell, J. H., 1995: Comparison of methods used to create estimate of air-freezing index. *Journal of Cold Regions Engineering*, 9(2): 64–74.
- Stocker, T., Qin, D., Plattner, G., Tignor, M., Allen, S., Boschung, J., Nauels, A., Xia, Y., Bex, B., and Midgley, B., 2013: *Climate Change 2013: The Physical Science Basis. Contribution of Working Group I to the Fifth Assessment Report of the Intergovernmental Panel on Climate Change (IPCC)*. New York: Cambridge University Press.
- Stow, D., Daeschner, S., Hope, A., Douglas, D., Petersen, A., Myneni, R., Zhou, L., and Oechel, W., 2003: Variability of the seasonally integrated normalized difference vegetation index across the north slope of Alaska in the 1990s. *International Journal of Remote Sensing*, 24(5): 1111–1117.
- Susan, S., 2007: *Climate Change 2007—The Physical Science Basis: Working Group I Contribution to the Fourth Assessment Report of the IPCC*. New York: Cambridge University Press.
- Vermette, S., and Christopher, S., 2008: Using the rate of accumulated freezing and thawing degree days as a surrogate for determining freezing depth in a temperate forest soil. *Middle States Geographer*, 41: 68–73.
- Wang, Q., Zhang, T.-j., Wu, J., Peng, X., Zhong, X., Mou, C., Wang, K., Wu, Q., and Cheng, G., 2013: Investigation on permafrost distribution over the upper reaches of the Heihe River in the Qilian Mountains. *Journal of Glaciology and Geocryology*, 35(1): 19–25.
- Willmott, C. J., and Robeson, S. M., 1995: Climatologically aided interpolation (CAI) of terrestrial air temperature. *International Journal of Climatology*, 15(2): 221–229.
- Wu, Q., and Liu, Y., 2004: Ground temperature monitoring and its recent change in Qinghai-Tibet Plateau. *Cold Regions Science and Technology*, 38(2): 85–92.
- Wu, T., Zhao, L., Li, S., Xie, C., Pang, Q., and Zhang, W., 2008: Freezing/thawing index variation during the last 40 year over the Tibet Plateau. In Proceedings, Ninth International Conference of Permafrost, Fairbanks, University of Alaska, 1969–1973.
- Wu, T., Wang, Q., Zhao, L., Batkhishig, O., and Watanabe, M., 2011: Observed trends in surface freezing/thawing index over the period 1987–2005 in Mongolia. *Cold Regions Science and Technology*, 69(1): 105–111.
- Xu, J., 2002: Mathematical methods in contemporary geography. *China Higher Education Press*, Beijing: 224–230.
- Zhang, J., Kang, E., Lan, Y., and Chen, R., 2003: Impact of climate change and variability on water resources in Heihe River Basin. *Journal of Geographical Sciences*, 13(3): 286–292.
- Zhang, T., and Stamnes, K., 1998: Impact of climatic factors on the active layer and permafrost at Barrow, Alaska. *Permafrost and Periglacial Processes*, 9(3): 229–246.
- Zhang, T., Frauenfeld, O. W., Serreze, M. C., Etringer, A., Oelke, C., McCreight, J., Barry, R. G., Gilichinsky, D., Yang, D., and Ye, H., 2005: Spatial and temporal variability in active layer thickness over the Russian Arctic drainage basin. *Journal of Geophysical Research: Atmospheres (1984–2012)*, 110(D16): doi <http://dx.doi.org/10.1029/2004JD005642>.
- Zhao, H.-y., Jiang, H., Wang, K.-l., and Yang, Y.-f., 2008: The surface thawing-freezing indexes along the Qinghai-Tibet Railway: analysis and calculation. *Journal of Glaciology and Geocryology*, 4014.

MS submitted 17 November 2013

MS accepted 29 July 2015